applied sciences

MDPI

Article

Optimal Unmanned Ground Vehicle—Unmanned Aerial Vehicle Formation-Maintenance Control for Air-Ground Cooperation

Jingmin Zhang [1,2], Xiaokui Yue [1,*], Haofei Zhang [2] and Tiantian Xiao [2]

[1] School of Astronautics, Northwestern Polytechnical University, Xi'an 710072, China; zjm_208suo@163.com
[2] No.208 Research Institute of China Ordnance Industries, Beijing 102202, China; jeamszhf@163.com (H.Z.); tessaxiao@163.com (T.X.)
* Correspondence: xkyue@nwpu.edu.cn

Abstract: This paper investigates the air–ground cooperative time-varying formation-tracking control problem of a heterogeneous cluster system composed of an unmanned ground vehicle (UGV) and an unmanned aerial vehicle (UAV). Initially, the structure of the UAV–UGV formation-control system is analyzed from the perspective of a cooperative combat system. Next, based on the motion relationship between the UAV–UGV in a relative coordinate system, the relative motion model between them is established, which can clearly reveal the physical meaning of the relative motion process in the UAV–UGV system. Then, under the premise that the control system of the UAG is closed-loop stable, the motion state of the UGV is modeled as an input perturbation. Finally, using a linear quadratic optimal control theory, a UAV–UGV formation-maintenance controller is designed to track the reference trajectory of the UGV based on the UAV–UGV relative motion model. The simulation results demonstrate that the proposed controller can overcome input perturbations, model-constant perturbations, and linearization biases. Moreover, it can achieve fast and stable adjustment and maintenance control of the desired UAV–UGV formation proposed by the cooperative combat mission planning system.

Keywords: UAV–UGV; cooperative engagement; optimal control; time-varying output formation; formation keeping

Citation: Zhang, J.;Yue, X.; Zhang, H. Xiao, T. Optimal Unmanned Ground Vehicle—Unmanned Aerial Vehicle Formation-Maintenance Control for Air-Ground Cooperation. *Appl. Sci.* **2022**, *12*, 3598. https://doi.org/10.3390/app12073598

Academic Editor: Yosoon Choi

Received: 6 March 2022
Accepted: 29 March 2022
Published: 1 April 2022

1. Introduction

In the wake of rapid development of information technology (IT), artificial intelligence (AI), and unmanned equipment, as well as their common application in the military field, the traditional combat style, in which each platform uses its own sensors and weapon systems to detect, track, and strike targets individually, can no longer meet the needs of digital warfare. As an emerging combat style, cooperative operations can organically link various geographically dispersed sensors, command and control systems, and weapons systems into a cross-platform information network. In this manner, it is possible to connect and share battlefield information, obtain real-time situational awareness of the battlefield, and improve the integrated combat effectiveness. Cooperative combat has received increasing academic attention in recent years. However, current research on cooperative operations mainly focuses on multi-missile cooperative guidance [1–3], formation control [4–6], formation design [7–9], path planning [10–12], and multitarget assignment [13–15]. Research on air–ground cooperative operations is currently lacking.

Unmanned aerial vehicles (UAVs) and unmanned ground vehicles (UGVs) are the two most representative objects in a cluster system. Although UAVs can quickly reconnoiter a wide area, they are limited by endurance and flight altitude, which prevents them from carrying out their given tasks in special environments. For UGVs, they are able to approach targets at a close range and have a high endurance, but are slower and have a limited

field of view. The advantages and disadvantages of UAVs and UGVs are summarized in Table 1. For a UAV–UGV cooperative formation, they can make full use of the advantages of spatial distribution, parallel execution of tasks, functional distribution, and fault tolerance, so that they can complement each other to compensate for the shortcomings of a single type of object and effectively improve the outcome of cooperative operations. For example, in the reconnaissance of complex terrain conditions, combat reconnaissance vehicles are often unable to detect effectively owing to obstacle blockages in the surrounding environment, and may even suffer communication losses between multiple vehicles. Introducing multiple UAVs to allow for formation control to achieve companion-flight cooperative reconnaissance can provide a large range of environmental information for the overall reconnaissance decisions of ground vehicles. Additionally, UAVs can be used as a communication relay in the case of ground communication obstacles to realize the complementary advantages and cooperation of the cluster system [16,17].

Table 1. Advantages and disadvantages of UAVs and UGVs.

Type of UAV		Advantages	Disadvantages
UAV	Small fixed-wing UAV	Fast velocity Wide field-of-view Excellent communication	Low load capacity Low observation accuracy
	Small rotary-wing UAV	Vertical takeoff landing Good reconnaissance	Low load capacity
	UGV	High load capacity Precise observation of ground targets	Small field-of-view Low velocity Weak communication

Based on this demand for engineering applications, many scholars have conducted research on the air–ground cooperative control between UAVs and UGVs. As an emerging research field, its theoretical knowledge and technical aspects involve the intersection of several disciplines and technical fields, such as embedded systems, aerodynamics, and control theory, which includes path tracking, formation clustering, automatic landing, and other research fields characterized by many research contents and difficulties [18,19]. This highlights that many problems need to be solved and explored in this area. In particular, the heterogeneity of UAVs and UGVs, for example, having different working fields, different physical models, and different technical indicators [20–22], poses new challenges to cooperative control between UAVs and UGVs [23,24].

Hence, this study investigates the air–ground cooperative time-varying formation-keeping control problem of a heterogeneous cluster system composed of a UGV and a UAV in the scenario of air–ground cooperative combat, which enables the UAV to track the motion trajectory of the UGV.

2. Related Work

Grocholsky et al. [25] proposed the use of an air–ground cooperative model to address the shortcomings of a single platform, e.g., the low accuracy of UAVs when locating ground targets and the narrow view of UGVs when observing distant obstacles. They designed a cooperative control framework and algorithm to search for and locate targets in a specified area, providing ideas for cooperative air–ground platforms to search for targets. Manyam et al. [26] considered the problem of communication constraints between two UAVs that cooperate to complete a mission. To address this issue, they proposed using UAVs to collect information and developed a branch-and-cut algorithm to solve the path-planning problem of UGVs and UAVs, offering a new idea for the cooperative path planning of UGVs and UAVs under communication constraints. In addition, they presented a cooperative reconnaissance and data-collection method for UGVs and UAVs.

To address the problem that the line of sight of a ground vehicle's sensors is limited by the geometry of the environment, Peterson et al. [27] presented a method to capture aerial images of the mission area using multi-rotors, construct a terrain map, and then navigate the ground robot to the destination. This method provides a theoretical and practical basis for the application of air–ground cooperative systems for cooperative navigation in outdoor environments.

However, the aforementioned studies on air–ground cooperation focus mostly on image transmission, map construction, and target localization, and do not consider the impact of UAV–UGV formation on the overall quality of cooperative operations. In fact, when UGVs and UAVs perform cooperative combat missions, formation adjustments are required, including initial formation generation, formation maintenance, contraction, expansion, and reconfiguration. Therefore, research on the formation control of UGVs and UAVs is of great significance, and can even affect whether a combat mission can be successfully completed.

UAVs and UGVs have completely different physical structures, and their established kinematic and dynamic models are entirely different. Moreover, UAVs perform three-dimensional movements in air, whereas UGVs perform two-dimensional movements on the ground. As a result, studying the time-varying formation-tracking control of heterogeneous cluster systems is a key problem to solve in cross-media heterogeneous collaboration, including air–ground collaboration, which has great theoretical research value and engineering significance.

Currently, common formation-control strategies include behavior-, virtual structure-, and consistency-based methods [28–30]. However, behavior-based formation methods rely on qualitative behavior rules, making it difficult to establish a quantitative model of the entire system. Consequently, such a method cannot guarantee the stability of the formation movement of an entire system. Virtual structure-based methods require centralized control by a central node, and cannot be implemented in a distributed manner. In addition, most existing methods can only achieve time-invariant formation configurations, whereas in practical applications, heterogeneous cluster systems must be able to dynamically adjust their formations in real time to cope with complex external environments and changes in tasks.

In the past, scholars have mainly used two methods to establish the relative motion models of UGVs and UAVs. One method is to directly analyze the geometric relationship of the motion of a single vehicle in a two-dimensional plane and establish a relative-motion model in a two-dimensional plane. The other is to derive the difference between the different vehicle positions in an inertial coordinate system and then obtain an expression of the relative motion state in the inertial space. This description cannot directly reflect the motion characteristics of UGVs and UAVs in a relative coordinate system, and their relative motion processes are insufficiently clear.

Based on the above research background, this study investigates the UAV–UGV formation-maintenance control problem for cooperative combat mission requirements. First, from the perspective of a UAV–UGV cooperative combat system, the architecture of the control system and the relationship between the sub-modules are analyzed. Subsequently, a relative motion model between the UGV and the UAV is established. The optimal UAV–UGV cooperative formation-maintenance control is then realized based on the proportional-integral (PI) optimal control theory. The main contributions of this study are as follows:

(1) By directly studying the motion relationship between a UGV and a UAV in a relative coordinate system, their relative equations of motion are established in three-dimensional space. It is possible to directly obtain the motion of the UGV and UAV in a relative three-dimensional coordinate system, thus clarifying the physical meaning of the relative motion between the two.
(2) The PI optimal control theory is used to design an optimal formation-maintenance controller that can overcome the constant relative-motion perturbations, as well as the

nonlinear-model linearization bias. This controller can potentially achieve fast and stable optimal control of UAV–UGV formation.

3. Relative Kinematic-Equation Building for UAV–UGV Formations

In this study, we investigate the UAV–UGV formation-maintenance control problem for cooperative combat mission requirements. Considering the actual motion state of a UGV as the input perturbation of the formation-maintenance controller, we assume that the control system of the UAV is closed-loop stable, i.e., the directions of the UAV velocity command, trajectory-inclination command, and trajectory-declination command can be stably followed. The three channels were set in the following first-order system [31]:

$$\begin{cases} \dot{V}_f = -\frac{1}{\tau_{vf}}\left(V_f - V_{fc}\right) \\ \dot{\theta}_f = -\frac{1}{\tau_{\theta f}}\left(\theta_f - \theta_{fc}\right) \\ \dot{\psi}_{vf} = -\frac{1}{\tau_{\psi vf}}\left(\psi_{vf} - \psi_{vfc}\right) \end{cases} \tag{1}$$

where τ_{vf} denotes the inertia time constant of the velocity control channel of the UAV, $\tau_{\theta f}$ denotes the inertia time constant of the track-inclination control channel of the UAV, $\tau_{\psi_{vf}}$ denotes the inertia time constant of the track-declination control channel of the UAV, V_f is the actual velocity magnitude of the UAV, θ_f is the actual inclination angle of the UAV, ψ_{vf} is the actual declination angle of the UAV, V_{fc} is the commanded velocity magnitude of the UAV, θ_{fc} is the commanded inclination angle of the UAV, and ψ_{vfc} is the commanded declination angle of the UAV.

To study the relative motion between the UGV and UAV, the following coordinate systems are first defined:

(1) Inertial coordinate system $O_1X_1Y_1Z_1$: The origin O_1 is located at a fixed point on the ground, the O_1X_1 axis points to the target, the O_1Y_1 axis is vertically upward, and the O_1Z_1 axis forms a right-handed coordinate system with the first two axes.

(2) Relative coordinate system $O_rX_rY_rZ_r$: The origin O_r is located at the center of mass of the UGV, the O_rX_r axis points in the direction of the UGV velocity, the O_rY_r axis is in the vertical plane perpendicular to the O_rX_r axis, and the O_rZ_r axis forms a right-handed coordinate system with the first two axes.

(3) Vehicle-body coordinate system $O_2X_2Y_2Z_2$: The origin O_2 is located at the center of mass of the UAV, the O_2X_2 axis points in the direction of the UAV velocity, the O_2Y_2 axis is in the vertical plane perpendicular to the O_2X_2 axis, and the O_2Z_2 axis forms a right-handed coordinate system with the first two axes.

In the relative coordinate system, according to Coriolis theory, the motions of the UGV and UAV are related as follows:

$$\frac{d\boldsymbol{r}}{dt} = \boldsymbol{V}_{fr} - \boldsymbol{V}_{lr} = \boldsymbol{V}_r + \boldsymbol{\omega} \times \boldsymbol{r} \tag{2}$$

where $\boldsymbol{r}$ is the relative radius vector between the UGV and UAV; $\boldsymbol{V}_{fr}$ and $\boldsymbol{V}_{lr}$ are the velocity vectors of the UAV and UGV in the relative coordinate system, respectively; $\boldsymbol{V}_r$ is the derivative of the radius vector $\boldsymbol{r}$ in the relative coordinate system; $\boldsymbol{\omega}$ is the angular velocity of rotation of the relative coordinate system in the inertial coordinate system.

To obtain the absolute velocity of the UGV and UAV in the relative coordinate system, the following transformation can be performed:

$$\begin{cases} \boldsymbol{V}_{ft} = \Phi_1^r \Phi_2^l \boldsymbol{V}_{f2} \\ \boldsymbol{V}_{lr} = \boldsymbol{V}_{l2} \end{cases} \tag{3}$$

where Φ_1^r is the conversion matrix from the inertial to the relative coordinate system; Φ_2^l is the conversion matrix from the UAV body coordinate system to the inertial coordinate system; $\boldsymbol{V}_{f2}$ is the velocity vector under the UAV body coordinate system; $\boldsymbol{V}_{l2}$ is the velocity

vector under the UGV body coordinate system. The values of each of these variables are as follows:

$$\Phi_1^r = \begin{bmatrix} \cos\theta_l \cos\psi_{vl} & \sin\theta_l & -\cos\theta_l \sin\psi_{vl} \\ -\sin\theta_l \cos\psi_{vl} & \cos\theta_l & \sin\theta_l \sin\psi_{vl}. \\ \sin\psi_{vl} & 0 & \cos\psi_{vl} \end{bmatrix} \tag{4}$$

$$\Phi_2^l = \begin{bmatrix} \cos\theta_f \cos\psi_{vf} & -\sin\theta_f \cos\psi_{vf} & \sin\psi_{vf} \\ \sin\theta_f & \cos\theta_f & 0 \\ -\cos\theta_f \sin\psi_{vf} & \sin\theta_f \sin\psi_{vf} & \cos\psi_{vf} \end{bmatrix} \tag{5}$$

$$\boldsymbol{V}_{l2} = \begin{bmatrix} V_l \\ 0 \\ 0 \end{bmatrix} \tag{6}$$

$$\boldsymbol{V}_{f2} = \begin{bmatrix} V_f \\ 0 \\ 0 \end{bmatrix} \tag{7}$$

where V_l denotes the velocity magnitude of the UGV in the inertial coordinate system; θ_l denotes the inclination angle of the UGV; ψ_{vl} denotes the deflection angle of the UGV; V_f is the velocity magnitude of the UAV in the inertial coordinate system; θ_f is the inclination angle of the UAV trajectory; ψ_{vf} is the deflection angle of the UAV trajectory. The relative velocities of the UGV and UAV in the relative coordinate system are expressed as follows:

$$\boldsymbol{V}_r = \begin{bmatrix} \dot{x} \\ \dot{y} \\ \dot{z} \end{bmatrix} \tag{8}$$

where x, y, and z are the components of the position vector $\boldsymbol{r}$ of the UAV along each axis in the relative coordinate system. The angular velocity of rotation $\boldsymbol{\omega}$ in the relative coordinate system with respect to the inertial space can be expressed as follows:

$$\boldsymbol{\omega} = \begin{bmatrix} \dot{\psi}_{vl} \sin\theta_l \\ \dot{\psi}_{vl} \cos\theta_l \\ \dot{\theta}_l \end{bmatrix} \tag{9}$$

Then, based on Equation (2), the following equation can be obtained:

$$\boldsymbol{V}_{fr} = \left(\boldsymbol{V}_{fr} - \boldsymbol{V}_{lr}\right) - \boldsymbol{\omega} \times \boldsymbol{r} \tag{10}$$

The relative motion relationship between the UAV and UGV in the three-dimensional plane can be obtained by combining Equations (2), (8), and (10).

$$\begin{cases} \dot{x} = V_f \cos\theta_f \cos\theta_l \cos\psi_e + V_f \sin\theta_f \sin\theta_l - V_l + y\dot{\theta}_l - z\dot{\psi}_{vl} \cos\theta_l \\ \dot{y} = -V_f \cos\theta_f \sin\theta_l \cos\psi_e + V_f \sin\theta_f \sin\theta_l - x\dot{\theta}_l + z\dot{\psi}_{vl} \sin\theta_l \\ \dot{z} = V_f \cos\theta_f \sin\psi_e - y\dot{\psi}_{vl} \sin\theta_l + x\dot{\psi}_{vl} \cos\theta_l \\ \psi_e = \psi_{vl} - \psi_{vf} \end{cases} \tag{11}$$

4. Optimal Control Modeling for the UAV–UGV Formation-Maintenance Controller

The design goal of the UAV–UGV formation-maintenance controller is to produce flight commands $V_{fc}, \theta_{fc}, \psi_{vf}$ for the UAV, to keep it at the desired relative distance from the UGV.

4.1. Linearization of the Relative Equations of Motion

During the UAV–UGV formation-maintenance process, assuming that θ_f, θ_l, and $\psi_e = \psi_{vl} - \psi_{vf}$ can be considered as small quantities, while considering the state of the UGV as an input quantity, Equation (11) is converted to

$$\begin{cases} \dot{x} = V_f + V_f\theta_f\theta_l - V_l + y\dot{\theta}_l - z\dot{\psi}_{vl} \\ \dot{y} = -V_f\theta_l + V_f\theta_f - x\dot{\theta}_l + z\dot{\psi}_{vl}\theta_l \\ \dot{z} = V_f\psi_e - y\dot{\psi}_{vl}\theta_l + x\dot{\psi}_{vl} \\ \psi_e = \psi_{vl} - \psi_{vf} \end{cases} \tag{12}$$

Using the small-perturbation linearization method, Equation (12) can be linearized as

$$\begin{cases} \dot{x} = \dot{\theta}_l y - \dot{\psi}_{vl} z + \left(1 + \theta_{f0}\theta_l\right) V_f + V_{f0}\theta_l\theta_f - V_l \\ \dot{y} = -\dot{\theta}_l x + \dot{\psi}_{vl}\theta_l z + \left(\theta_{f0} - \theta_l\right) V_f + V_{f0}\theta_f \\ \dot{z} = \dot{\psi}_{vl} x - \dot{\psi}_{vl}\theta_l y + \left(\psi_{vl} - \psi_{vf0}\right) V_f - V_{f0}\psi_{vf} \end{cases} \tag{13}$$

where v_{f0}, θ_{f0}, and ψ_{vf0} are the state equilibrium points selected during linearization.

Describing Equation (13) as a state-space form (SSF) yields

$$\begin{cases} \dot{\boldsymbol{X}} = \boldsymbol{A}\boldsymbol{X} + \boldsymbol{B}\boldsymbol{U} + \tilde{\boldsymbol{B}}\boldsymbol{W} \\ \boldsymbol{Y} = \boldsymbol{C}\boldsymbol{X} \end{cases} \tag{14}$$

where

$$\boldsymbol{A} = \begin{bmatrix} 0 & \dot{\theta}_L & -\dot{\psi}_{vl} \\ -\dot{\theta}_l & 0 & \theta_L\dot{\psi}_{vl} \\ \dot{\psi}_{vl} & -\theta_L\dot{\psi}_{vl} & 0 \end{bmatrix} \tag{15}$$

$$\boldsymbol{B} = \begin{bmatrix} 1 + \theta_{f0}\theta_l & V_{f0}\theta_l & 0 \\ \theta_{f0} - \theta_l & V_{f0} & 0 \\ \psi_{vl} - \psi_{vf0} & 0 & -V_{f0} \end{bmatrix} \tag{16}$$

$$\boldsymbol{C} = \begin{bmatrix} 1 & 0 & 0 \\ 0 & 1 & 0 \\ 0 & 0 & 1 \end{bmatrix} \tag{17}$$

$$\tilde{\boldsymbol{B}} = \begin{bmatrix} 1 \\ 0 \\ 0 \end{bmatrix} \tag{18}$$

where $\boldsymbol{X} = \begin{bmatrix} x & y & z \end{bmatrix}^T$ denotes the state variable; $\boldsymbol{U} = \begin{bmatrix} V_f & \theta_f & \psi_{vf} \end{bmatrix}^T$ denotes the control variable of the formation controller, which is the motion state of the UAV; $\boldsymbol{Y} = \begin{bmatrix} x & y & z \end{bmatrix}^T$ denotes the output variable; the perturbation variable is the velocity $\boldsymbol{W} = \boldsymbol{V}_l$ of the UGV.

4.2. Optimal Formation-Maintenance Controller Design

According to the state-space equations of the system, the controller design problem for UAV–UGV formations is a non-zero set-point output-regulation problem with constant or slow-varying perturbations. Two steps can be taken to solve this problem: the first step is to design an optimal output regulation controller that can solve constant or slow varying perturbations. The second step is to design an optimal controller to solve the non-zero set-point problem so that the UAV–UGV formation can be stably maintained at the desired formation position.

4.2.1. PI Optimal Formation-Maintenance Controller Design

The perturbed system of type shown in Equation (14), with constant or slowly varying values, can be overcome using a PI type of control, similar to that in classical control theory. This section analyzes the problem of designing PI optimal controllers with zero values as the output regulation set points.

First, the system perturbation is transformed into a perturbation of the control input, at which point, system (14) becomes

$$\dot{\boldsymbol{X}} = \boldsymbol{A}\boldsymbol{X} + \boldsymbol{B}(\boldsymbol{U} + \tilde{\boldsymbol{W}}) \tag{19}$$

where $\tilde{\boldsymbol{W}}$ denotes the transformed form of the original system perturbation. The following equation can be obtained from system (14):

$$\tilde{\boldsymbol{W}} = \boldsymbol{B}^{-1}\tilde{\boldsymbol{B}}\boldsymbol{W} \tag{20}$$

Next, we design the PI optimal controller of the perturbed system (19), which can be augmented as

$$\begin{cases} \dot{\boldsymbol{X}}_1 = \boldsymbol{A}_1\boldsymbol{X}_1 + \boldsymbol{B}_1\boldsymbol{U}_1 \\ \boldsymbol{Y}_1 = \boldsymbol{C}_1\boldsymbol{X}_1 \end{cases} \tag{21}$$

where

$$\boldsymbol{X}_1 = \begin{bmatrix} \boldsymbol{X} \\ \boldsymbol{U} + \tilde{\boldsymbol{W}} \end{bmatrix} \tag{22}$$

$$\boldsymbol{A}_1 = \begin{bmatrix} \boldsymbol{A} & \boldsymbol{B} \\ \boldsymbol{0} & \boldsymbol{0} \end{bmatrix} \tag{23}$$

$$\boldsymbol{B}_1 = \begin{bmatrix} \boldsymbol{0} \\ \boldsymbol{I} \end{bmatrix} \tag{24}$$

$$\boldsymbol{C}_1 = \begin{bmatrix} \boldsymbol{I} & \boldsymbol{0} \end{bmatrix} \tag{25}$$

For the augmented system (21), the quadratic performance index is given as

$$J = \int_{t_0}^{t_f} \left[\boldsymbol{X}_1^T \boldsymbol{Q}_1 \boldsymbol{X}_1 + \boldsymbol{U}_1^T \boldsymbol{R}_1 \boldsymbol{U}_1 \right] dt \tag{26}$$

where $\boldsymbol{Q}_1$ is the state-regulation power-coefficient matrix of the augmented system and $\boldsymbol{R}_1$ is the control energy power coefficient matrix of the augmented system. When the system (21) is controllable, according to optimal control theory, the minimum optimal control to achieve the quadratic performance index (26) is

$$\boldsymbol{U}_1^* = -\boldsymbol{R}_1^{-1}\boldsymbol{B}_1^T\boldsymbol{P}\boldsymbol{X}_1 \tag{27}$$

Let us further analyze the quadratic performance index (26). Based on the composition of the state variable $\boldsymbol{X}_1$, $\boldsymbol{Q}_1$ can be decomposed as follows:

$$\boldsymbol{Q}_1 = \begin{bmatrix} \boldsymbol{Q} & \boldsymbol{0} \\ \boldsymbol{0} & \boldsymbol{R} \end{bmatrix} \tag{28}$$

Then, we can have

$$\boldsymbol{X}_1^T\boldsymbol{Q}_1\boldsymbol{X}_1 = \boldsymbol{X}^T\boldsymbol{Q}\boldsymbol{X} + (\boldsymbol{U} + \tilde{\boldsymbol{W}})^T\boldsymbol{R}(\boldsymbol{U} + \tilde{\boldsymbol{W}}) \tag{29}$$

where $\boldsymbol{Q}$ is the state-regulation power-coefficient matrix of the original system (14) and $\boldsymbol{R}$ is its control energy power coefficient matrix.

According to system (14), we can have

$$\boldsymbol{X}^T\boldsymbol{Q}\boldsymbol{X} = \boldsymbol{X}^T\boldsymbol{C}^T\boldsymbol{Q}_Y\boldsymbol{C}\boldsymbol{X} = \boldsymbol{Y}^T\boldsymbol{Q}_Y\boldsymbol{Y} \tag{30}$$

where $\boldsymbol{Q}_Y$ is the output regulation power-coefficient matrix of the original system.

The optimal quadratic state-regulation performance index described in Equation (26) becomes the optimal quadratic output-regulation problem.

$$J = \int_{t_0}^{t_f} \left[\boldsymbol{Y}^T \boldsymbol{Q}_Y \boldsymbol{Y} + (\boldsymbol{U} + \tilde{\boldsymbol{W}})^T \boldsymbol{R} (\boldsymbol{U} + \tilde{\boldsymbol{W}}) + \boldsymbol{U}_1^T \boldsymbol{R}_1 \boldsymbol{U}_1 \right] dt \tag{31}$$

Assuming that the perturbation $\tilde{\boldsymbol{W}}$ is a slow variable, it follows that

$$\dot{\tilde{\boldsymbol{W}}} = \boldsymbol{0} \tag{32}$$

Then, we have

$$\boldsymbol{U}_1 = \dot{\boldsymbol{U}} \tag{33}$$

Thus, the quadratic optimal output performance index of the system (21) can be described as

$$J = \int_{t_0}^{t_f} \left[\boldsymbol{Y}^T \boldsymbol{Q}_Y \boldsymbol{Y} + (\tilde{\boldsymbol{U}} + \tilde{\boldsymbol{W}})^T \boldsymbol{R} (\tilde{\boldsymbol{U}} + \tilde{\boldsymbol{W}}) + \dot{\tilde{\boldsymbol{U}}}^T \boldsymbol{R}_1 \dot{\tilde{\boldsymbol{U}}} \right] dt \tag{34}$$

For the optimal control quantity (27), the following equation can be obtained by combining it with (33):

$$\boldsymbol{U}_1^* = \dot{\tilde{\boldsymbol{U}}}^* = -\boldsymbol{R}_1^{-1} \boldsymbol{B}_1^T \boldsymbol{P} \boldsymbol{X}_1 \tag{35}$$

where $\boldsymbol{P}$ is the minimum solution of the Riccati optimal control equation for achieving the performance index in Equation (26). Then, Equation (35) can be further expanded as

$$\begin{aligned} \dot{\tilde{\boldsymbol{U}}}^* &= -\boldsymbol{R}_1^{-1} \begin{bmatrix} \boldsymbol{0} \\ \boldsymbol{I} \end{bmatrix} \begin{bmatrix} \boldsymbol{P}_{11} & \boldsymbol{P}_{12} \\ \boldsymbol{P}_{21} & \boldsymbol{P}_{22} \end{bmatrix} \begin{bmatrix} \boldsymbol{X} \\ \tilde{\boldsymbol{U}}^* + \tilde{\boldsymbol{W}} \end{bmatrix} \\ &= -\boldsymbol{R}_1^{-1} \boldsymbol{P}_{21} \boldsymbol{X} - \boldsymbol{R}_1^{-1} \boldsymbol{P}_{22} \left(\tilde{\boldsymbol{U}}^* + \tilde{\boldsymbol{W}} \right) \end{aligned} \tag{36}$$

The above equation is an indicator of the minimum optimal control amount required to achieve the zero-valued set point in Equation (26).

4.2.2. Design of Non-Zero Set-Point OPTIMAL Controllers

To maintain the output quantity $\boldsymbol{Y} = \begin{bmatrix} x & y & z \end{bmatrix}^T$ at a non-zero set point, the state and control input of the system at the steady state must also be non-zero. The optimal control input based on Equation (35) should take the following form.

$$\dot{\tilde{\boldsymbol{U}}}^* = -\boldsymbol{R}_1^{-1} \boldsymbol{B}_1^T \boldsymbol{P} \boldsymbol{X}_1 + \boldsymbol{U}_0' = -\boldsymbol{K} \boldsymbol{X}_1 + \boldsymbol{U}_0' \tag{37}$$

where $\boldsymbol{U}_0'$ is the additional control quantity that stabilizes the non-zero set point. The output equation of the augmented system is

$$\boldsymbol{Y} = \boldsymbol{C}_1 \boldsymbol{X}_1 \tag{38}$$

From the expanded state $\boldsymbol{X}_1$, the augmented system is

$$\boldsymbol{X}_1 = \begin{bmatrix} x \\ y \\ z \\ V_f + \tilde{W}(1) \\ \tilde{W}(2) \\ \tilde{W}(3) \end{bmatrix} \tag{39}$$

To ensure that the output of the augmented system is consistent with the output of the original system, the output matrix of the augmented system is set to

$$\boldsymbol{C}_1 = \begin{bmatrix} 1 & 0 & 0 & 0 & 0 & 0 \\ 0 & 1 & 0 & 0 & 0 & 0 \\ 0 & 0 & 1 & 0 & 0 & 0 \end{bmatrix} \tag{40}$$

By substituting the control quantity (37) into the augmented system (21), we obtain

$$\dot{\boldsymbol{X}}_1 = (\boldsymbol{A}_1 - \boldsymbol{B}_1\boldsymbol{K})\boldsymbol{X}_1 + \boldsymbol{B}_1\boldsymbol{U}_0' \tag{41}$$

Because the closed-loop system (41) is asymptotically stable, the following condition should exist at steady state:

$$\lim_{t\to\infty} \dot{\boldsymbol{X}}_1(t) = 0 \tag{42}$$

This leads to the following asymptotically stable form.

$$\boldsymbol{0} = (\boldsymbol{A}_1 - \boldsymbol{B}_1\boldsymbol{K})\boldsymbol{X}_{10} + \boldsymbol{B}_1\boldsymbol{U}_0' \tag{43}$$

where $\boldsymbol{X}_{10}$ is the steady-state value of state $\boldsymbol{X}_1$.

If all eigenvalues of matrix $(\boldsymbol{A}_1 - \boldsymbol{B}_1\boldsymbol{K})$ are in the left half-complex plane, then $(\boldsymbol{A}_1 - \boldsymbol{B}_1\boldsymbol{K})$ is a non-singular matrix, and the following equation can be obtained by combining with Equation (43).

$$\boldsymbol{X}_{10} = -(\boldsymbol{A}_1 - \boldsymbol{B}_1\boldsymbol{K})^{-1}\boldsymbol{B}_1\boldsymbol{U}_0' \tag{44}$$

Then, based on Equation (38), the relationship between the non-zero set point $\boldsymbol{Y}_{10}^*$ and the steady-state value $\boldsymbol{X}_{10}$ of state $\boldsymbol{X}_1$ is obtained as

$$\boldsymbol{Y}_{10}^* = \boldsymbol{C}_1\boldsymbol{X}_{10} \tag{45}$$

Finally,

$$\dot{\boldsymbol{U}}^* = -\boldsymbol{R}_1^{-1}\boldsymbol{B}_1^{\mathrm{T}}\boldsymbol{P}\boldsymbol{X}_1 + \left[\boldsymbol{C}_1\left(-\boldsymbol{B}_1\boldsymbol{R}_1^{-1}\boldsymbol{B}_1^{\mathrm{T}}\boldsymbol{P} - \boldsymbol{A}_1\right)^{-1}\boldsymbol{B}_1\right]^{-1}\boldsymbol{Y}_{10}^* \tag{46}$$

can be used to achieve optimal control of the relative motion system between the UGV and the UAV, as described in Equation (14); thus, maintaining the UAV–UGV formation in the desired state.

5. Simulation Analysis

In this section, we describe the numerical simulations performed for the UAV–UGV formation-maintenance control system consisting of a UGV with a given motion state, a UAV with a first-order stability control system, and an optimal maintenance controller. The inertial time constants of the three channels of the UGV and UAV are assumed to be $\tau_{vf} = 3$ s, $\tau_{\theta f} = 1$ s, and $\tau_{\psi_{vf}} = 1$ s. The initial positions of the UAV and UGV in the inertial coordinate system are chosen as $(-5, 20, 10)$ m and $(0, 0, 0)$ m, respectively. It is assumed that the UAV–UGV formation moves for 150 s, and the simulation step size is taken to be 0.01 s. Under the action of Equation (43), the entire motion of the UAV is adjusted and maintained from the initial position to the desired position at $(-5, 20, 10)$ m. In all simulations, the required control system power coefficient matrix in Equation (34) appears as the matrices shown in Equation (47). Considering the feasible motion envelope of the

UAV, limits are set for the control amount of the formation controller and commanded motion state of the UAV, as shown in Equation (52).

$$\boldsymbol{Q}_y = \begin{bmatrix} 4 & 0 & 0 \\ 0 & 6 & 0 \\ 0 & 0 & 6 \end{bmatrix}, \boldsymbol{R} = \begin{bmatrix} 1 & 0 & 0 \\ 0 & 1 & 0 \\ 0 & 0 & 1 \end{bmatrix}, \boldsymbol{R}_1 = \begin{bmatrix} 1 & 0 & 0 \\ 0 & 1 & 0 \\ 0 & 0 & 1 \end{bmatrix} \tag{47}$$

To verify the effectiveness of the proposed UGV–UAV formation-maintenance controller, we set two cases in which the UGV adopts different motion modes. The motion of the UGV is set as in Equations (48) to (51). The simulation results are shown in Figures 1 and 2.

case 1:

$$V_l(t) = \begin{cases} 2 + \sin(0.1t)\ \mathrm{m/s}, 0 \leq t < 50\ \mathrm{s} \\ 2\ \mathrm{m/s}, 50 \leq t < 100\ \mathrm{s} \\ 2 + \sin(0.1t)\ \mathrm{m/s}, 100 \leq t < 150\ \mathrm{s}. \end{cases} \tag{48}$$

$$\begin{cases} \theta_l(t) = 0\ \mathrm{rad} \\ \psi_{vl}(t) = 0.5\cos(0.1t + 0.7728)\ \mathrm{rad} \end{cases} \tag{49}$$

case 2:

$$V_l(t) = \begin{cases} 1.5\ \mathrm{m/s}, 0 \leq t < 50\ \mathrm{s} \\ 2 + \sin(0.1t)\ \mathrm{m/s}, 50 \leq t < 100\ \mathrm{s} \\ 1.5\ \mathrm{m/s}, 100 \leq t < 150\ \mathrm{s} \end{cases} \tag{50}$$

$$\begin{cases} \theta_l(t) = 0\ \mathrm{rad} \\ \psi_{vl}(t) = 0.2\sin(0.15t + 0.5523)\ \mathrm{rad} \end{cases} \tag{51}$$

$$\begin{cases} 1\ \mathrm{m/s} \leqslant V_{fc} \leqslant 3\ \mathrm{m/s} \\ -15^\circ \leqslant \theta_{fc} \leqslant 25^\circ \\ -80^\circ \leqslant \psi_{vfc} \leqslant 80^\circ \end{cases} \tag{52}$$

It can be seen from Figures 1 and 2 that under the control command in Equation (46), the UGV can guide the UAV to fly at a fixed altitude in accordance with the specified motion, which results in the maintenance of a fixed formation in the three-dimensional plane. In addition, the velocity and declination angle commands of the UVA vary slightly and reasonably without the jitter vibration phenomenon, which satisfies the constraints of the laws of physics. Moreover, the motion of the UGV perturbs the UAV–UGV formation-maintenance control. As the UGV changes its motion form at 50 and 100 s, the motion trajectory of the UAV fluctuates at the corresponding moments. Nevertheless, it can be quickly stabilized at the desired motion state using a formation-maintenance controller. In case 1, the maximum values of the motion state errors of the UAV in the X_r, Y_r, and Z_r directions are 1.2 m , 0 m, and 1.8 m, respectively. In Case 2, the maximum values of the motion state errors of the UAV in the X_r, Y_r, and Z_r directions are 0.6 m, 0 m, and 0.6 m, respectively.

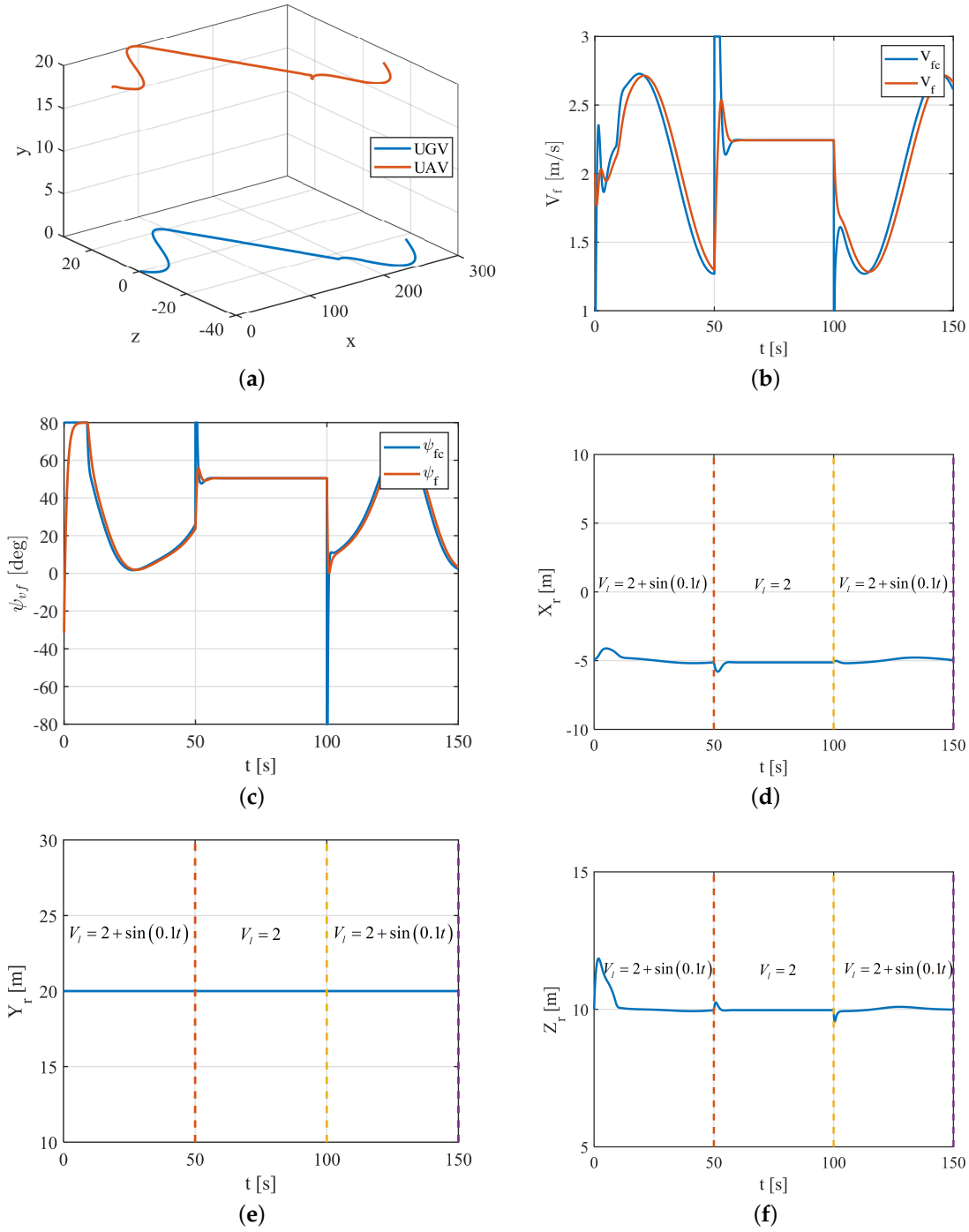

Figure 1. Simulation results of case 1. (**a**) Three-dimensional motion trajectory of UGV and UAV; (**b**) velocity of UAV; (**c**) deflection angle of UAV; (**d**) motion trajectory in X_r-axis direction; (**e**) motion trajectory in Y_r-axis direction; (**f**) motion trajectory in Z_r-axis direction.

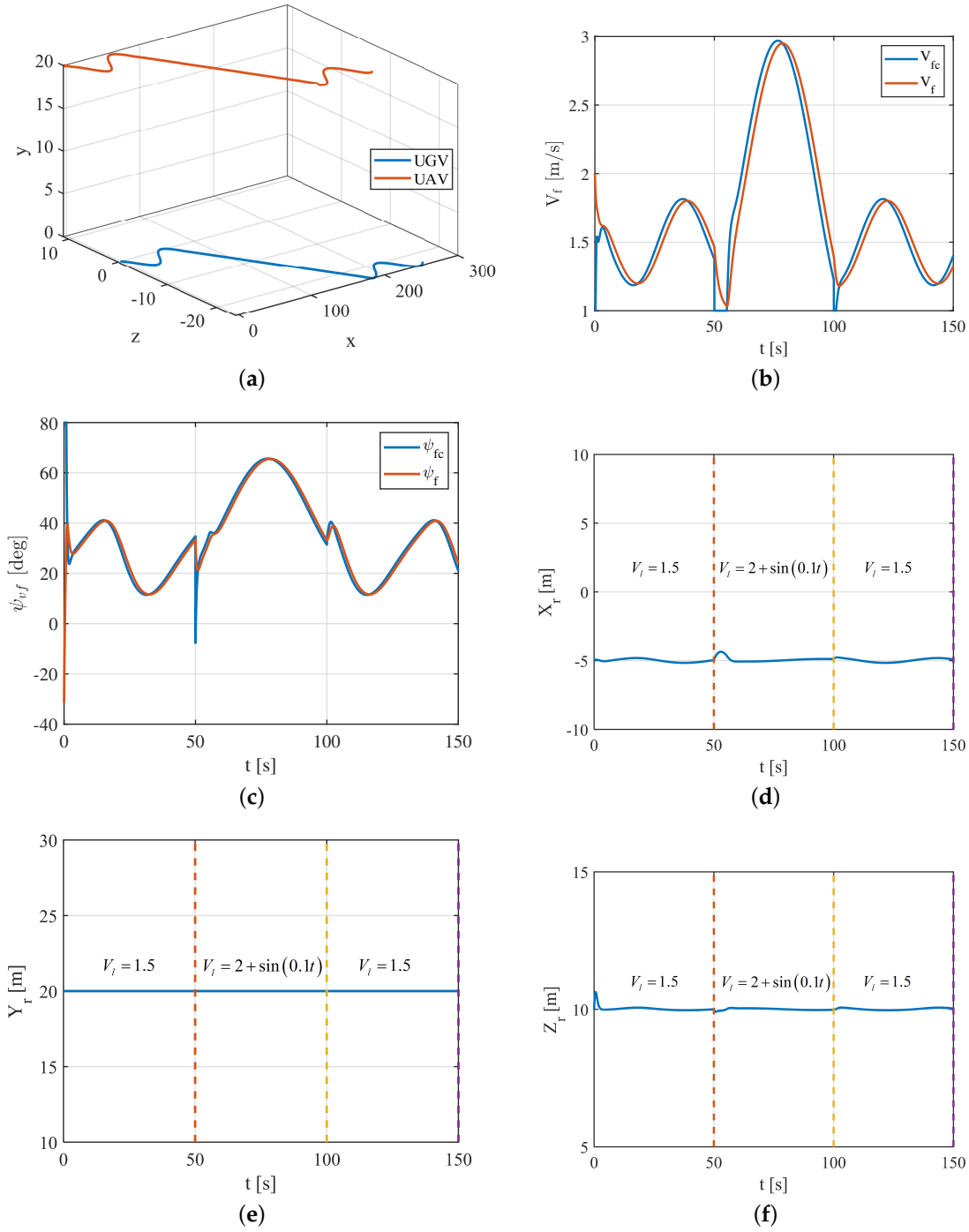

Figure 2. Simulation results of case 2. (**a**) Three-dimensional motion trajectory of UGV and UAV; (**b**) velocity of UAV; (**c**) deflection angle of UAV; (**d**) motion trajectory in X_r-axis direction; (**e**) motion trajectory in Y_r-axis direction; (**f**) motion trajectory in Z_r-axis direction.

6. Conclusions

This study analyzed the structure of the UAV–UGV formation motion control system and the relationship between the subsystems. A UAV–UGV formation–maintenance controller was designed based on the optimal control theory. In addition, simulations were performed for the UAV–UGV formation-maintenance control system, including a UGV with a given motion state, a UAV with a first-order stability-control system, and an optimal maintenance controller. The following conclusions were drawn.

(1) The physical significance of the UAV–UGV relative-motion model, based directly on the UAV motion relationship in the relative coordinate system, was clear.
(2) The optimal UAV–UGV formation-maintenance controller designed in this study had quadratic optimal properties for the UAV–UGV relative-motion state, as well as the formation-control energy. The controller could overcome the constant perturbation of the UAV–UGV relative motion caused by the velocity of the UGV. The optimal UAV–UGV formation-maintenance controller could overcome the given motion state of the UGV as an input perturbation, while the UGV performed a prolonged motion.
(3) Within the flight envelope of the UAV–UGV formation, the optimal UAV–UGV formation-maintenance controller was able to overcome the errors introduced by the linearization of a nonlinear model.

Author Contributions: The contributions of the authors are the following; conceptualization: all authors; methodology: H.Z. and X.Y.; software: T.X.; writing: J.Z.; investigation: T.X. All authors have read and agreed to the published version of the manuscript.

Funding: The authors appreciate the financial support from the National Natural Science Foundation of China (NSFC) (62173274), Natural Science Foundation of Shaanxi Province (2020JQ-219), and Aviation Fund (20200001053005).

Institutional Review Board Statement: Not applicable.

Informed Consent Statement: Not applicable.

Data Availability Statement: All data used during the study appear in the submitted article.

Conflicts of Interest: All of the authors declare that they have no known competing financial interests or personal relationships that could appear to influence the work reported in this paper.

References

1. Song, J.; Song, S.; Xu, S. Three-dimensional cooperative guidance law for multiple missiles with finite-time convergence. *Aerosp. Sci. Technol.* **2017**, *67*, 193–205. [CrossRef]
2. Liu, S.; Yan, B.; Liu, R.; Dai, P.; Yan, J.; Xin, G. Cooperative guidance law for intercepting a hypersonic target with impact angle constraint. *Aeronaut. J.* **2022**, 1–19.
3. Wang, C.; Ding, X.; Wang, J.; Shan, J. A robust three-dimensional cooperative guidance law against maneuvering target. *J. Frankl. Inst.* **2020**, *357*, 5735–5752. [CrossRef]
4. Chen, C.P.; Yu, D.; Liu, L. Automatic leader-follower persistent formation control for autonomous surface vehicles. *IEEE Access* **2018**, *7*, 12146–12155. [CrossRef]
5. Lu, Y.; Zhang, G.; Sun, Z.; Zhang, W. Adaptive cooperative formation control of autonomous surface vessels with uncertain dynamics and external disturbances. *Ocean Eng.* **2018**, *167*, 36–44. [CrossRef]
6. Kuriki, Y.; Namerikawa, T. Consensus-based cooperative formation control with collision avoidance for a multi-UAV system. In Proceedings of the 2014 American Control Conference, Linz, Austria, 15–17 July 2014; pp. 2077–2082.
7. Liu, S.; Huang, F.; Yan, B.; Zhang, T.; Liu, R.; Liu, W. Optimal Design of Multimissile Formation Based on an Adaptive SA-PSO Algorithm. *Aerospace* **2022**, *9*, 21. [CrossRef]
8. Lin, X.; Shi, X.; Li, S. Optimal cooperative control for formation flying spacecraft with collision avoidance. *Sci. Prog.* **2020**, *103*. [CrossRef]
9. Ousingsawat, J.; Campbell, M.E. Optimal cooperative reconnaissance using multiple vehicles. *J. Guid. Control Dyn.* **2007**, *30*, 122–132. [CrossRef]
10. Bellingham, J.S.; Tillerson, M.; Alighanbari, M.; How, J.P. Cooperative path planning for multiple UAVs in dynamic and uncertain environments. In Proceedings of the 41st IEEE Conference on Decision and Control, Las Vegas, NV, USA, 10–13 December 2002; Volume 3, pp. 2816–2822.
11. Yu, H.; Meier, K.; Argyle, M.; Beard, R.W. Cooperative path planning for target tracking in urban environments using unmanned air and ground vehicles. *IEEE/ASME Trans. Mechatron.* **2014**, *20*, 541–552.
12. Gang, L.; Song-Yang, L.; Dong-Feng, T.; Zhi-Chao, Z. Research status and progress on anti-ship missile path planning. *Acta Autom. Sin.* **2013**, *39*, 347–359.
13. Liu, S.; Liu, W.; Huang, F.; Yin, Y.; Yan, B.; Zhang, T. Multitarget allocation strategy based on adaptive SA-PSO algorithm. *Aeronaut. J.* **2022**, 1–13.
14. Guo, J.; Hu, G.; Guo, Z.; Zhou, M. Evaluation Model, Intelligent Assignment and Cooperative Interception in Multi-missile and Multi-target Engagement. *IEEE Trans. Aerosp. Electron. Syst.* **2022**.

15. Poore, A.P.; Rijavec, N. A Lagrangian relaxation algorithm for multidimensional assignment problems arising from multitarget tracking. *SIAM J. Optim.* **1993**, *3*, 544–563. [CrossRef]
16. Lakas, A.; Belkhouche, B.; Benkraouda, O.; Shuaib, A.; Alasmawi, H.J. A framework for a cooperative UAV–UGV system for path discovery and planning. In Proceedings of the 2018 International Conference on Innovations in Information Technology (IIT), Al Ain, United Arab Emirates, 18–19 November 2018; pp. 42–46.
17. Arbanas, B.; Ivanovic, A.; Car, M.; Orsag, M.; Petrovic, T.; Bogdan, S. Decentralized planning and control for UAV–UGV cooperative teams. *Auton. Robot.* **2018**, *42*, 1601–1618. [CrossRef]
18. Yu, K.; Budhiraja, A.K.; Buebel, S.; Tokekar, P. Algorithms and experiments on routing of unmanned aerial vehicles with mobile recharging stations. *J. Field Robot.* **2019**, *36*, 602–616. [CrossRef]
19. Harik, E.H.C.; Guérin, F.; Guinand, F.; Brethé, J.F.; Pelvillain, H. UAV–UGV cooperation for objects transportation in an industrial area. In Proceedings of the 2015 IEEE International Conference on Industrial Technology (ICIT), Seville, Spain, 17–19 March 2015; pp. 547–552.
20. Rodriguez-Ramos, A.; Sampedro, C.; Bavle, H.; De La Puente, P.; Campoy, P. A deep reinforcement learning strategy for UAV autonomous landing on a moving platform. *J. Intell. Robot. Syst.* **2019**, *93*, 351–366. [CrossRef]
21. Palafox, P.R.; Garzón, M.; Valente, J.; Roldán, J.J.; Barrientos, A. Robust visual-aided autonomous takeoff, tracking, and landing of a small UAV on a moving landing platform for life-long operation. *Appl. Sci.* **2019**, *9*, 2661. [CrossRef]
22. Ghamry, K.A.; Kamel, M.A.; Zhang, Y. Cooperative forest monitoring and fire detection using a team of UAVs-UGVs. In Proceedings of the 2016 International Conference on Unmanned Aircraft Systems (ICUAS), Arlington, VA, USA, 7–10 June 2016; pp. 1206–1211.
23. Kamel, M.A.; Ghamry, K.A.; Zhang, Y. Real-time fault-tolerant cooperative control of multiple UAVs-UGVs in the presence of actuator faults. *J. Intell. Robot. Syst.* **2017**, *88*, 469–480. [CrossRef]
24. Khaleghi, A.M.; Xu, D.; Wang, Z.; Li, M.; Lobos, A.; Liu, J.; Son, Y.J. A DDDAMS-based planning and control framework for surveillance and crowd control via UAVs and UGVs. *Expert Syst. Appl.* **2013**, *40*, 7168–7183. [CrossRef]
25. Grocholsky, B.; Keller, J.; Kumar, V.; Pappas, G. Cooperative air and ground surveillance. *IEEE Robot. Autom. Mag.* **2006**, *13*, 16–25. [CrossRef]
26. Manyam, S.G.; Casbeer, D.W.; Sundar, K. Path planning for cooperative routing of air-ground vehicles. In Proceedings of the 2016 American Control Conference (ACC), Boston, MA, USA, 6–8 July 2016; pp. 4630–4635.
27. Peterson, J.; Chaudhry, H.; Abdelatty, K.; Bird, J.; Kochersberger, K. Online aerial terrain mapping for ground robot navigation. *Sensors* **2018**, *18*, 630. [CrossRef] [PubMed]
28. Beard, R.W.; Lawton, J.; Hadaegh, F.Y. A coordination architecture for spacecraft formation control. *IEEE Trans. Control Syst. Technol.* **2001**, *9*, 777–790. [CrossRef]
29. Takahashi, H.; Nishi, H.; Ohnishi, K. Autonomous decentralized control for formation of multiple mobile robots considering ability of robot. *IEEE Trans. Ind. Electron.* **2004**, *51*, 1272–1279. [CrossRef]
30. Oh, K.K.; Park, M.C.; Ahn, H.S. A survey of multi-agent formation control. *Automatica* **2015**, *53*, 424–440. [CrossRef]
31. Cui, N.; Wei, C.; Guo, J.; Zhao, B. Research on missile formation control system. In Proceedings of the 2009 International Conference on Mechatronics and Automation, Changchun, China, 9–12 August 2009; pp. 4197–4202.